Journal of Solid State Electrochemistry (2023) 27:2645–2658
https://doi.org/10.1007/s10008-023-05562-2

ORIGINAL PAPER

Application of nitrogen-doped multi-walled carbon nanotubes decorated with gold nanoparticles in biosensing

Nikos G. Tsierkezos[1] · Emma Freiberger[1] · Uwe Ritter[1] · Stefan Krischok[2] · Fabian Ullmann[2] · J. Michael Köhler[3]

Received: 14 April 2023 / Revised: 31 May 2023 / Accepted: 1 June 2023 / Published online: 8 June 2023

Abstract

Novel films consisting of nitrogen-doped multi-walled carbon nanotubes (N-MWCNTs) were fabricated by means of chemical vapor deposition technique and decorated with gold nanoparticles (AuNPs) possessing diameter of 14.0 nm. Electron optical microscopy analysis reveals that decoration of N-MWCNTs with AuNPs does not have any influence on their bamboo-shaped configuration. The electrochemical response of fabricated composite films, further denoted as N-MWCNTs/AuNPs, towards oxidation of dopamine (DA) to dopamine-o-quinone (DAQ) in the presence of ascorbic acid (AA) and uric acid (UA) was probed in real pig serum by means of cyclic voltammetry (CV) and square wave voltammetry (SWV). The findings demonstrate that N-MWCNTs/AuNPs exhibit slightly greater electrochemical response and sensitivity towards DA/DAQ compared to unmodified N-MWCNTs. It is, consequently, obvious that AuNPs improve significantly the electrochemical response and detection ability of N-MWCNTs. The electrochemical response of N-MWCNTs/AuNPs towards DA/DAQ seems to be significantly greater compared to that of conventional electrodes, such as platinum and glassy carbon. The findings reveal that N-MWCNTs/AuNPs could serve as powerful analytical sensor enabling analysis of DA in real serum samples.

Keywords Ascorbic acid · Dopamine · Electrochemical biosensors · Gold nanoparticles · Nitrogen-doped multi-walled carbon nanotubes · Pig serum · Uric acid

Introduction

Sensors based on multi-walled carbon nanotubes (MWCNTs) were extensively applied in electrochemical analysis since they provide great electrochemically active area, high electrical conductivity, extremely high reactivity and selectivity, and enhanced electrochemical stability [1]. Furthermore, MWCNTs exhibit improved electric transport properties as well as electro-catalytic activity, and thus are capable to reduce the overpotentials and thereby to improve the currents of redox systems [2–4]. In addition, MWCNTs display high sensitivity and detection capability, and consequently, they improve the reaction rate and amplify the stability and reproducibility of the electrode's response [5].

The modification of MWCNTs with metal nanoparticles, such as gold nanoparticles (AuNPs), seems to be quite promising for the enhancement of their electrochemical performance. Namely, it is well known that such a combination improves significantly the electrochemical response of MWCNT-based sensors towards redox systems. For instance, it has been observed that although the electrochemical activity of either MWCNTs or AuNPs films (individually) exhibits a good response towards numerous redox systems, several biomolecules do not undergo electrocatalysis on these materials. To overcome this difficulty, various modification processes were carried out in order to prepare composite films consisting of both MWCNTs and AuNP materials. Thus, according to literature reports, MWCNT-based electrodes modified with AuNPs were applied in electroanalysis for the determination of various redox systems. In those studies, both MWCNTs and AuNP materials were used for the modification of conventional electrodes, such as carbon paste [6], glassy carbon [7, 8], and platinum [9], and relatively high

✉ Nikos G. Tsierkezos
nikos.tsierkezos@tu-ilmenau.de

1 Institute of Chemistry and Biotechnology, Department of Chemistry, Ilmenau University of Technology, Weimarer Straße 25, 98693 Ilmenau, Germany

2 Institute of Physics and Institute of Micro- and Nanotechnologies MacroNano, Ilmenau University of Technology, PF 100565, 98684 Ilmenau, Germany

3 Institute of Chemistry and Biotechnology, Department of Physical Chemistry and Micro Reaction Technology, Ilmenau University of Technology, Ilmenau, Germany

detection ability and sensitivity were observed for these modified electrode systems.

Dopamine or 2-(3,4-dihydroxyphenyl)ethylamin (further abbreviated as DA) is a member of the catecholamine family and one of the best-known neurotransmitters that activates five known types of dopamine receptors (D1-D5) and their variants [10]. DA has a wide variety of functions in the brain, including important roles in pleasure, behavior, understanding, controlled movement, motivation, sleep, mood, attention, working memory, and learning. DA is strongly associated with the pleasure system in the brain, and its release provides feelings of enjoyment and supports the activities, which result from these feelings. Disorders in DA levels cause declines in neurocognitive functions like memory, attention, and problem-solving. Furthermore, the lack of DA results in Parkinson's disease, schizophrenia, and other related disorders [1, 13]. Over the past several years, there has been great interest in developing sensitive and simple analytical methods, such as spectroscopy and chromatography, for the determination of DA and the diagnosis of some diseases caused by DA deficiency [14–18] However, it is well known that in clinical medicine the development of an electro-analytical method for studying electron transfer processes is quite advantageous. Since DA is an electrochemically active compound, it can be easily analyzed in unknown biological samples by means of electrochemical methods based on its anodic oxidation. As was already suggested [19], the oxidation of DA can be in general characterized as a two-electron transfer process that leads to the formation of corresponding di-ketone, namely dopamine-o-quinone (further referred as DAQ), according to the following reaction:

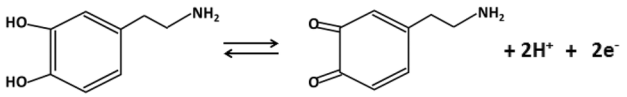

However, detailed schemes published in the literature suggested that DA is firstly oxidized to DAQ that is transformed to more oxidizable 5,6-dihydroxyindoline or leucodopaminechrome, which is further oxidized to aminochrome or dopaminechrome [19].

Numerous studies for electrochemical determination of DA on various electrodes including also those based on nanostructured carbon materials were already carried out and reported in the literature [20–38]. In those studies, a variety of novel electrode materials with greatly enhanced electrochemical performance was successfully used for the analysis of DA in unknown biological samples. However, a literature survey demonstrates that comprehensive studies of DA on N-MWCNT/AuNP-based electrodes were not carried out so far. Thus, there is a pressing need to gain insight into the electrochemical behavior of such composite materials in biosensing.

In the current manuscript, we report our recent studies on the electrochemical response of nitrogen-doped multi-walled carbon nanotubes (N-MWCNTs) modified with gold nanoparticles (AuNPs) possessing a diameter of 14.0 nm, further denoted as N-MWCNTs/AuNPs, towards dopamine (DA) in the presence of ascorbic acid (AA) and uric acid (UA) in real pig serum samples. The N-MWCNTs were grown directly on an oxidized porous silicon wafer upon decomposition of acetonitrile (source of carbon and nitrogen) in the presence of ferrocene (catalyst) by means of a chemical vapor deposition technique. The fabricated N-MWCNT-based films were characterized by means of X-ray photoelectron spectroscopy (XPS), scanning electron microscopy (SEM), and transmission electron microscopy (TEM) combined with energy dispersive X-ray spectroscopy (EDX). For the electrochemistry measurements, the cyclic voltammetry (CV) and square wave voltammetry (SWV) techniques were applied. It is well known that CV and SWV are the most widely used voltammetry techniques for studying redox reactions since they provide information on the steps involved in electrochemical processes with only a modest expenditure of time and effort in the acquisition and interpretation of data. To our knowledge, there has been no report so far regarding the effect of AuNPs-modification on the electrochemical response of N-MWCNTs, directly grown on silicon/silicon oxide wafers, towards DA oxidation. In the present research work, we are going to demonstrate that the decoration of surfaces of carbon nanotubes with AuNPs improves significantly their electrochemical activity for the detection of DA in the presence of ascorbic acid (AA) and uric acid (UA) in real pig serum samples.

Experimental

Chemicals and solutions

Acetonitrile (> 99.9%), ferrocene (> 98.0%), and dopamine (> 99.0%) were purchased from Sigma-Aldrich, while L(+)-ascorbic acid (> 99.7%) and uric acid (> 98.0%) were obtained from Merck. The pig serum was purchased from BIO&SELL (Germany). The phosphate buffer solution (pH 7.0) was prepared using monosodium phosphate and its conjugate base, disodium phosphate, both purchased from Merck. All reagents were of analytical grade and were used without any further purification. Initial electrochemistry studies were carried out to determine the best BS-to-PBS ratio for the electrochemistry measurements (Fig. S1; ESM). According to obtained results, the ratio of 1:10 (BS to PBS) seems to be quite optimum for the electrochemical analysis. The solutions of DA of desired concentrations in the range of 0.010–0.350 mM were prepared directly in an electrochemical

cell with the addition of proper volumes of stock solutions of DA into pig serum mixed with phosphate buffer solution in a ratio of 1:10. The concentration of AA (0.500 mM) and UA (0.100 mM) was kept constant in all measurements.

Fabrication of N-MWCNTs

The N-MWCNT-based films were synthesized by means of the chemical vapor deposition (CVD) technique onto an oxidized porous silicon wafer using acetonitrile as carbon and nitrogen source materials in the presence of ferrocene that serves as catalyst [39]. The scheme of the pyrolysis apparatus and experimental details for the application of the CVD technique for the synthesis of carbon nanotubes were reported in previously published articles [40–42].

Synthesis of AuNPs

Colloidal noble AuNPs possessing a diameter of 14.0 nm were fabricated using the photochemical segmented flow technique [43, 44]. A representative scheme of apparatus used for the fabrication of AuNPs is shown in Fig. S2 (ESM). The setup was built up of three PC-controlled syringe pumps, PTFE-tubing with an inner diameter of 0.5 mm, standard fluid connectors, and one 4-port-manifold (both made of polyether ether ketone). The segmented flow technique is suitable for the micro continuous-flow synthesis of plasmonic nanoparticles with high-size homogeneity and for tuning nanoparticle properties. It causes a narrow residence time distribution for all volume elements of the reactant mixture under the UV ray and a high reproducibility of the fluid motion in this range. The noble AuNPs were prepared using the metal salt solution with a concentration of 1.0 mM. The salt solution was mixed with the polyvinylpyrrolidone/photoinitiator solution (PVP/PI) in a 4-port-manifold and segmented with perfluoromethyldecalin (PP9). The PVP/PI solution was previously prepared from PVP solution (2 wt%) and 2-hydroxy-4′-(2-hydroxyethoxy)-2-methylpropiophenone solution (3.0 mM). The nucleation starts with the irradiation of the segments in the photo initiation element (length of focus of 2 mm; irradiation time of 135 ms). A diagram showing the size distribution for AuNPs is shown in Fig. S3 (ESM).

Decoration of N-MWCNTs with AuNPs

For the modification with AuNPs, the N-MWCNT-based films were initially immersed in an aqueous solution of sodium citrate (2.5 mM) and left in the solution for about 10 min. After this treatment, the films were dried in the air for about 2 h at the room temperature. Afterwards, the fabricated colloidal solution of AuNPs was dropped onto treated N-MWCNT films using a micropipette and left for drying under room conditions. Finally, the prepared N-MWCNT/AuNP composite films were carefully washed with distilled water and dried in the air for about 24 h. For the construction of N-MWCNTs and N-MWCNT/AuNP-based working electrodes, the films were connected to platinum wire by using a silver conducting coating. Once the silver coating was dried (~ 24 h), the silver conducting part of the films was fully covered with a varnish protective coating. Once the protective coating was dried (~ 12 h), the films were ready to be used as working electrodes for the electrochemistry measurements. The various stages for the construction of working electrodes used in the present work are shown in Fig. S4 (ESM). It must be mentioned that the N-MWCNTs and N-MWCNT/AuNP-based films were quite stable and no detachment of the electrode's contacting part occurred during the electrochemistry measurements.

Instrumentation

All electrochemistry measurements were performed on the electrochemical working station Zahner (IM6/6EX, Germany). The results were analyzed by means of Thales software (version 4.15). A three-electrode system consisting of either N-MWCNTs or N-MWCNT/AuNP-based working electrode, platinum auxiliary electrode, and Ag/AgCl (saturated KCl) reference electrode was used for electrochemistry measurements. Details regarding electrochemistry measurements were reported in the previously published article [45]. The morphology and elemental composition of N-MWCNTs/AuNPs were examined by scanning electron microscope (Zeiss ULTRA Plus SEM) and transmission electron microscope equipped with an energy dispersive X-ray spectrometer (FEI Titan S/TEM 80-300 kV) [46, 47]. The chemical composition of fabricated N-MWCNTs was studied by means of X-ray photoelectron spectroscopy in normal emission using an ultra-high vacuum (UHV) system equipped with a Physical Electronics 10–610 X-ray source in combination with an Omicron XM1000 monochromator for the generation of monochromated Al Kα radiation ($h\nu = 1486.7$ eV) and a 7 channel EA125 hemispherical electron analyzer operated at constant pass energy of 13 eV for detailed and 35 eV for survey spectra. More details regarding XPS analysis were reported in the previously published article [48]. Surfaces were bombarded for 5 min by Ar^+ ions with an energy of 3 keV to avoid the investigation of adsorbates on the surface.

Results and discussion

XPS analysis of N-MWCNTs/AuNPs

The XPS spectrum recorded for N-MWCNT/AuNP composite film is shown in Fig. 1. For comparison reasons, XPS spectrum

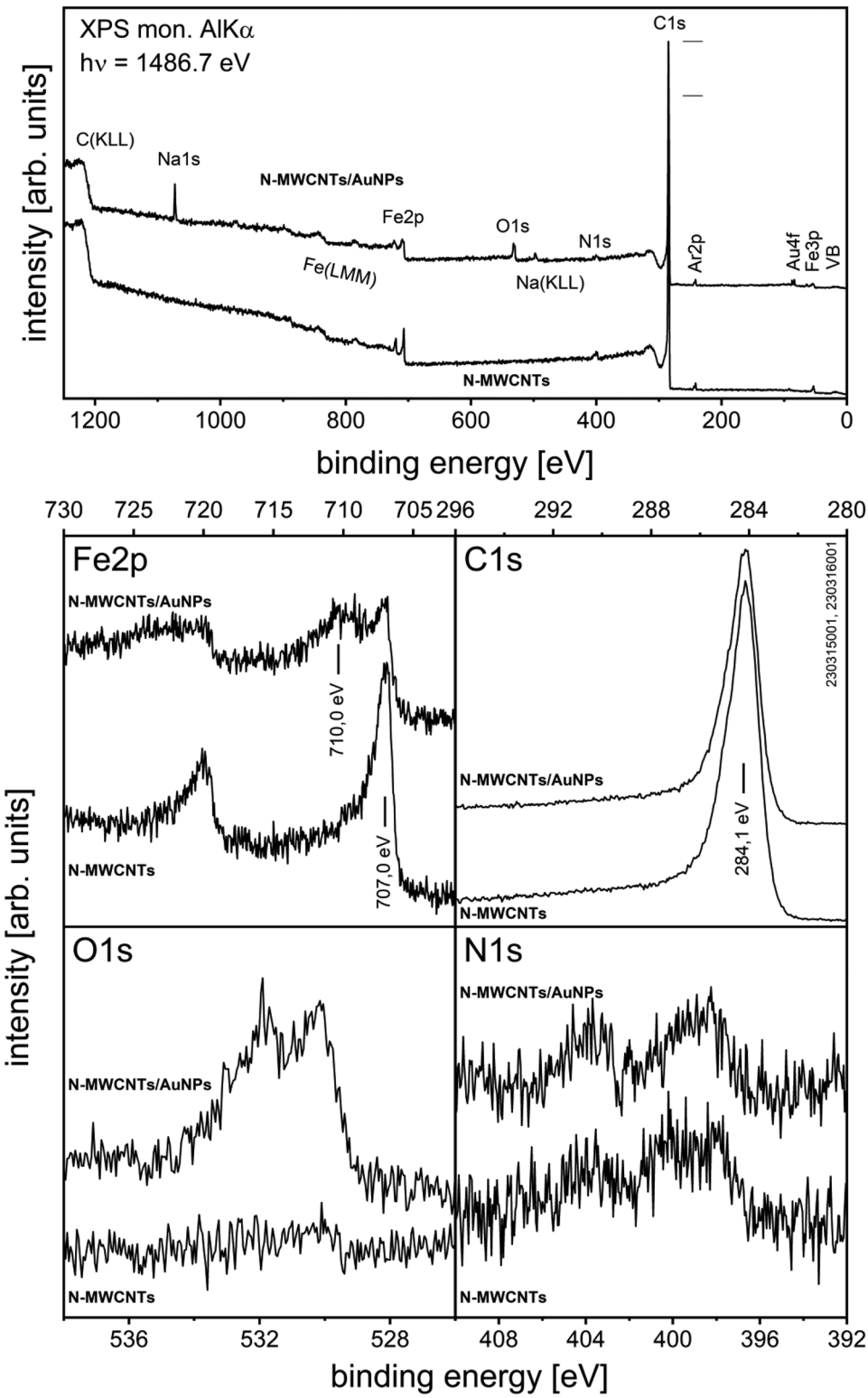

Fig. 1 XPS survey spectra recorded as well as Fe2p, C1s, O1s, and N1s detailed spectra of N-MWCNTs and N-MWCNTs/AuNPs after sputtering with Ar^+ for 5 min with an energy of 5 keV

for undecorated N-MWCNTs was recorded and presented along with that of N-MWCNTs/AuNPs in Fig. 1. In the detailed spectra of the C1s orbital, the typical shape of the photo electron peak of MWCNTs is found and confirms the production of MWCNTs. The XPS-analysis results are reported in Table 1. Nitrogen, iron, and carbon were found in composite films of N-MWCNTs. Composite films of N-MWCNTs/AuNPs show additional appearances of oxygen, gold, and sodium. The

Table 1 Elemental % composition of N-MWCNTs and N-MWCNTs/AuNPs determined based on quantitative analysis of the XPS core level signal assuming a homogeneous distribution of all components. The total percentage uncertainty of the measurements lies at about 2.5%

Material	C	Fe	N	O	Au	Na
N-MWCNTs	96.8	0.9	2.2	0.0	0.0	0.0
N-MWCNTs/AuNPs	92.8	1.1	2.4	2.8	0.1	0.9

findings confirm that the carbon nanotubes are doped with nitrogen.

SEM and TEM/EDX analysis of N-MWCNTs/AuNPs

The SEM and TEM techniques were applied to investigate the morphology of synthesized N-MWCNT/AuNP composite films. Representative SEM and TEM images taken for N-MWCNTs/AuNPs (14.0 nm) are shown in Fig. 2. SEM and TEM images of undecorated N-MWCNT films were already published in a previous article [49]. The low magnification SEM images exhibit that the surface of N-MWCNT/AuNP-based film is quite homogeneous and mainly free from amorphous carbon. The thickness of N-MWCNT/AuNP-based films was estimated to lie in the range of 26–28 μm. The high magnification SEM micrographs exhibit that the packing organization and thus the arrangement of aligned carbon nanotubes on an oxidized silicon substrate are quite enhanced. This observation is attributed to the bamboo-shaped configuration of carbon nanotubes that are doped with nitrogen [50]. In addition, the SEM micrographs reveal that the deposited metal nanoparticles are dispersed homogeneously onto the surface of N-MWCNTs and that no agglomeration of metal nanoparticles occurs. TEM analysis confirms that the N-MWCNTs modified with AuNPs possess the so-called bamboo structure similar to unmodified N-MWCNTs, commonly observed for carbon nanotubes that incorporate nitrogen into their structure. Furthermore, the TEM images demonstrate that the bamboo structure of modified N-MWCNTs shows no significant changes upon decoration with AuNPs compared to unmodified N-MWCNTs. In addition, the TEM images reveal that the metal nanoparticles get deposited on the side walls of nanotubes and are dispersed homogeneously all over the surface of the carbon nanotubes. Besides, the TEM images confirm that the carbon nanotubes contain a small amount of iron catalyst residue. Combined TEM/EDX analysis of AuNPs deposited on N-MWCNTs/AuNPs confirms that the observed nanoparticles consist of high-purity gold (Fig. S5; ESM).

Electrochemical response of N-MWCNTs/AuNPs towards DA

For characterizing the electrochemical performance of fabricated novel N-MWCNTs/AuNPs towards oxidation of DA to DAQ, CVs were recorded in PBS (pH 7.0) and BS/PBS (1:10) at various scan rates (in the range of 0.02–0.12 $V \bullet s^{-1}$) and analyte concentrations (in the range of 0.010–0.350 mM). For comparison reasons, electrochemistry experiments were also carried out on unmodified N-MWCNTs under similar conditions. Representative CVs recorded for oxidation of DA on N-MWCNTs and N-MWCNTs/AuNPs in PBS and BS/PBS (1:10) are shown in Fig. 3. The curves showing the variation of oxidation peak current density with a concentration of DA on N-MWCNTs and N-MWCNTs/AuNPs in PBS, BS, and BS/PBS (1:10) are presented in inset plots of Fig. 3. The electrochemical parameters determined for DA/DAQ redox system on N-MWCNTs and N-MWCNTs/AuNPs in PBS and BS/PBS are presented in Table 2.

It is apparent from CV curves that there is an electrochemical response of both N-MWCNTs and N-MWCNTs/AuNPs towards oxidation of DA to DAQ that leads to the appearance of two couples of oxidation and reduction CV-waves demonstrating the occurrence of more than one redox process involving redox behavior of DA. The mechanism of the electro-oxidation of DA in physiological pH is somehow complicated, and thus, there is confusion concerning this redox process. However, detailed schemes showing the processes upon electro-oxidation of DA published in the literature demonstrate that DA is firstly oxidized to the diketone dopamine-o-quinone (DAQ) that is transformed to the more oxidizable leucodopaminechrome, which is further oxidized to dopaminechrome [51, 52]. Specifically, upon the electrochemical treatment of DA, one chemical and two redox procedures take place. The first redox process concerns the facile oxidation of DA to DAQ via two-electron transfer that leads to the anodic CV-peak at about + 0.240 V (vs. Ag/AgCl) and the inverse procedure, namely the reduction of DAQ to DA which results in the cathodic CV-peak at about + 0.200 V (vs. Ag/AgCl). The electrochemically formed DAQ undergoes nucleophilic attack of amine in the side chain, and after an intra-molecular proton transfer, a generation of short-lived species occurs. Under the influence of water, the short-lived species undergoes an elimination reaction to form the stable aromatic phenolate anion [53]. Finally, upon protonation of phenolate anion, the electro-active 5,6-dihydroxyindoline or leucodopaminechrome (further referred to as DHI) is formed that can be oxidized at about −0.180 V (vs. Ag/AgCl) via elimination of two electrons to form aminochrome or dopaminechrome (further referred to as AC). Thus, the cathodic CV peak that

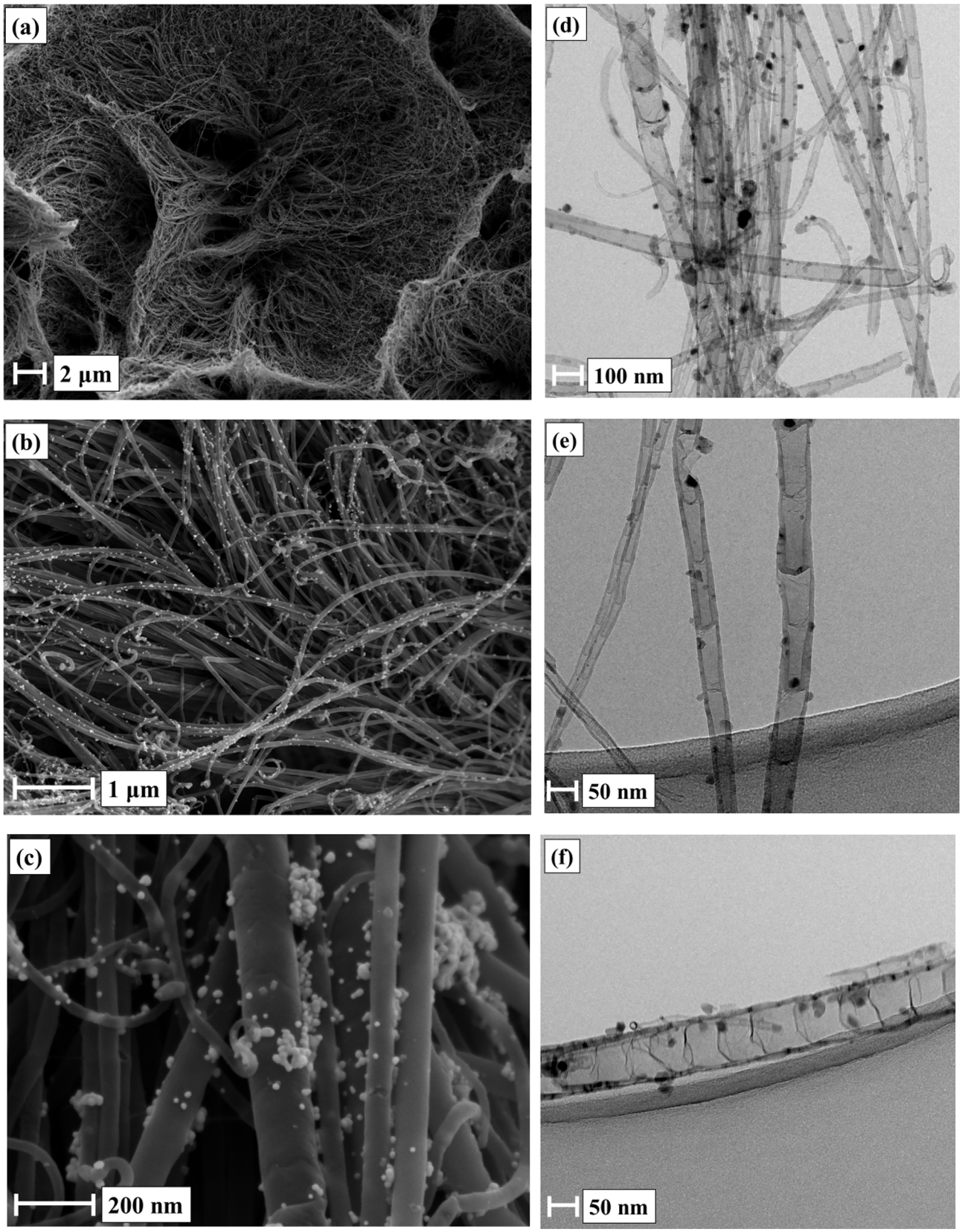

Fig. 2 SEM (**a**, **b**, **c**) and TEM (**d**, **e**, **f**) micrographs taken for N-MWCNT/AuNP (14.0 nm) composite film

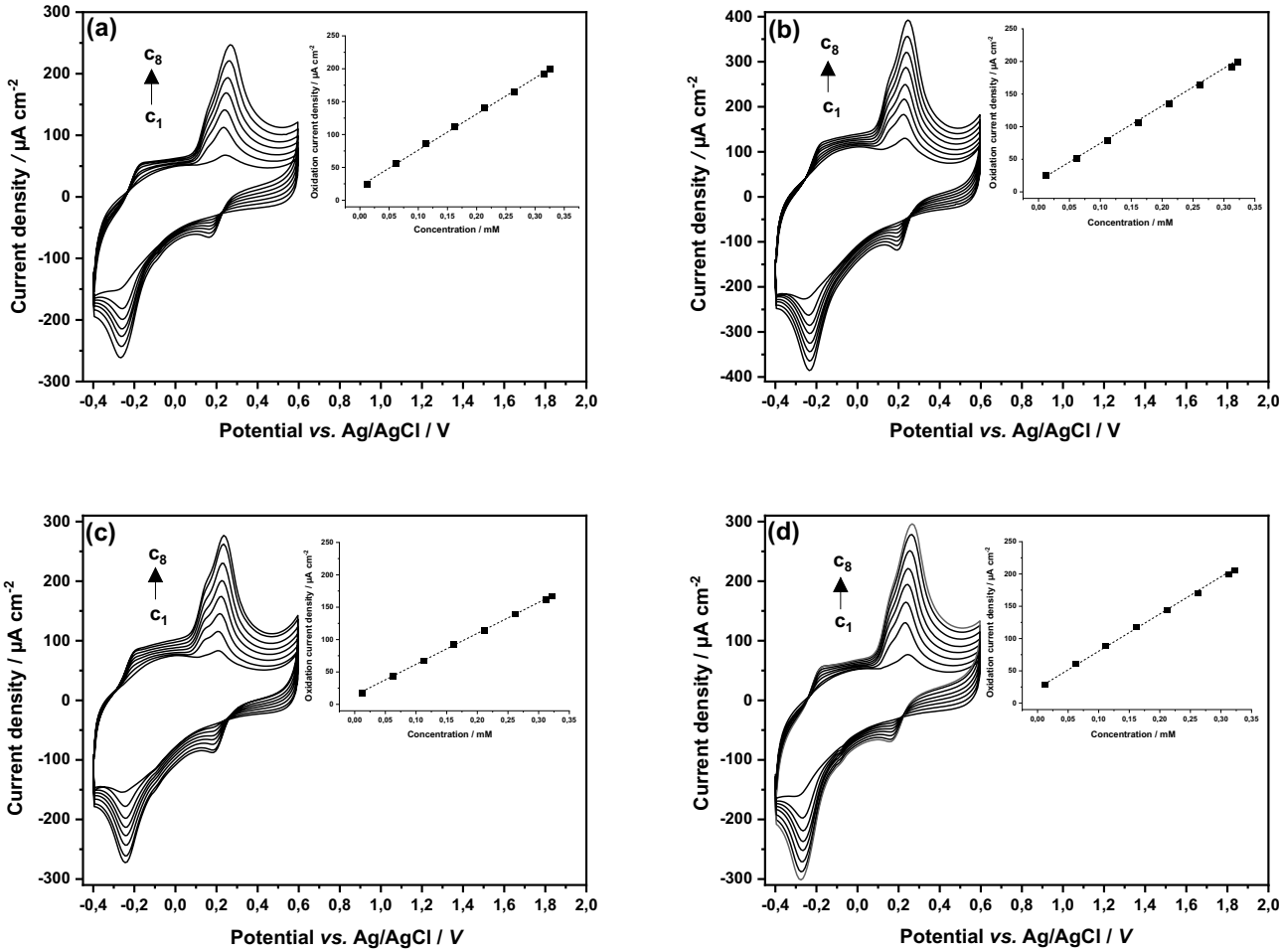

Fig. 3 CVs recorded for various concentrations of DA in range of 0.010–0.350 mM in PBS (**a**, **b**), BS/PBS (1:10) (**c**, **d**) on N-MWCNTs (**a**, **c**) and N-MWCNTs/AuNPs (**b**, **d**) at the scan rate of 0.02 V·s^{-1}. The insets exhibit the variation of oxidation peak current density with concentration of DA observed in recorded CVs

lies at about −0.270 V (vs. Ag/AgCl) can be attributed to the inverse process, namely to the reduction of AC to DHI.

As can be seen in the CV curves shown in Fig. 3, both N-MWCNTs and N-MWCNT/AuNP films exhibit irreversible redox response towards DA/DAQ in both PBS and BS/PBS solvent media. Consequently, it is noticeable that the cathodic peak current density is much smaller than the anodic peak current density (thus $i_p^{ox}/i_p^{red} > 1$) (Table 2) showing that only a part of the initial DA, which still remains in the DAQ form, can be regenerated, while the rest is consumed due to the competing chemical reaction and finally reduced at a more negative potential (−0.270 V vs. Ag/AgCl). It is, therefore, obvious that the kinetics of DA/DAQ redox couple on N-MWCNTs and N-MWCNTs/AuNPs is not enough fast, and consequently, the coupled chemical reaction for the conversion of DAQ to DHI prevails over its reduction to DA.

The anodic and cathodic peak potential separation (ΔE_p) for DA/DAQ redox couple on N-MWCNTs and N-MWCNTs/AuNPs in PBS was estimated as $\Delta E_p = 0.050$ V and $\Delta E_p = 0.032$ V, respectively (Table 2). The determined ΔE_p value on N-MWCNTs appears to be greater than the expected ΔE_p value for the two-electron transfer process (~ 0.059/n in V) demonstrating slow electron transfer kinetics on this particular film [54]. However, the ΔE_p value on N-MWCNTs/AuNPs seems to approach the expected theoretical ΔE_p value showing a faster electron transfer kinetic process on this particular electrode. The greater ΔE_p reflects slower kinetics of electron transfer reaction, specifically, ΔE_p is expected to be inversely related to heterogeneous electron transfer rate constant (k_s). The k_s values for DA/DAQ redox system on N-MWCNTs and N-MWCNTs/AuNPs were determined by means of electrochemical absolute rate relation: $\psi = (D_o/D_R)^{a/2} k_s (n\pi F v D_o/RT)^{-1/2}$, where ψ is the kinetic parameter, a the charge transfer coefficient, D_o, D_R the diffusion coefficients of oxidized and reduced species, respectively, and n the number of electrons involved in redox reaction [55,

Table 2 Anodic peak potential (E_p^{ox}), cathodic peak potential (E_p^{red}), half-wave potential ($E_{1/2}$), anodic and cathodic peak potential separation (ΔE_p), anodic and cathodic peak current ratio (i_p^{ox}/i_p^{red}), heterogeneous electron transfer rate constant (k_s), lower limit of detection (*LOD*), and sensitivity (*S*) for DA/DAQ on N-MWCNTs and N-MWCNT/AuNP composite films in PBS and BS/PBS (1:10)

Parameters	N-MWCNTs		N-MWCNTs/AuNPs	
	PBS	BS/PBS	PBS	BS/PBS
E_p^{ox} / V[a]	0.245 ± 0.003	0.240 ± 0.003	0.237 ± 0.003	0.225 ± 0.003
E_p^{red} / V[a]	0.195 ± 0.003	0.195 ± 0.003	0.205 ± 0.003	0.195 ± 0.003
$E_{1/2}$ / V[ab]	0.220 ± 0.006	0.218 ± 0.006	0.221 ± 0.006	0.210 ± 0.006
ΔE_p / V	0.050 ± 0.006	0.045 ± 0.006	0.032 ± 0.006	0.030 ± 0.006
i_p^{ox}/i_p^{red}	3.3 ± 0.2	3.7 ± 0.2	3.8 ± 0.2	3.9 ± 0.2
k_s / cm·s^{-1}[c]	0.14 ± 0.02	0.25 ± 0.03	1.76 ± 0.04	2.54 ± 0.05
LOD / μM[df]	1.90 ± 0.07	2.50 ± 0.09	1.60 ± 0.06	1.90 ± 0.06
S / A·M^{-1}·cm^{-2}[d]	0.434 ± 0.011	0.416 ± 0.011	0.565 ± 0.015	0.548 ± 0.014
S / A·M^{-1}·cm^{-2}[e]	0.369 ± 0.007	0.349 ± 0.006	0.480 ± 0.009	0.466 ± 0.009

[a]All potentials are reported *versus* Ag/AgCl (saturated KCl) reference electrode

[b]The $E_{1/2}$ values were determined as the average values of E_p^{ox} and E_p^{red}

[c]The k_s values were determined from obtained ΔE_p considering that the diffusion coefficient of DA is 6.0×10^{-6} cm^2·s^{-1} [70]

[d]The *LOD* and *S* values were estimated by means of CV technique in concentration range of 0.010–0.350 mM

[e]The *S* values were estimated by means of SWV technique in concentration range of 0.010–0.300 mM

[f]The *LOD* were estimated at signal-to-noise ratio of 3 (*S*/*N* = 3)

56]. The maximum error in the estimation of rate constants lies at about 2.0%. Consequently, the kinetic parameter k_s determined by means of electrochemical absolute rate relation for DA/DAQ on N-MWCNTs ($k_s = 0.14$ cm·s^{-1}) seems to be more than ten times smaller compared to k_s estimated on N-MWCNTs/AuNPs ($k_s = 1.76$ cm·s^{-1}). These findings demonstrate the important role that plays modification of N-MWCNTs with AuNPs in the improvement of the film's electrochemical response (kinetic). Furthermore, the kinetic of DA/DAQ on N-MWCNTs ($k_s = 0.25$ cm·s^{-1}) and N-MWCNTs/AuNPs ($k_s = 2.54$ cm·s^{-1}) in BS/PBS solutions seems to be slightly faster indicating that the fabricated composite films can be successfully applied in real serum samples.

It is interesting that the electrochemical kinetics of DA/DAQ on N-MWCNTs and N-MWCNTs/AuNPs estimated in the present work appears to be considerably faster compared to that reported in the literature for the same redox system on either bare glassy carbon electrode ($k_s = 0.39 \times 10^{-3}$ cm·s^{-1}) [57] or boron-doped diamond film (2.08×10^{-5}–6.60×10^{-5} cm·s^{-1}) [58]. Consequently, based on this evidence, the final conclusion that can be made is that the electrochemical response of N-MWCNTs and N-MWCNTs/AuNPs towards DA/DAQ is rather fast.

Slightly higher oxidation and reduction current density values were obtained on N-MWCNTs/AuNPs compared to unmodified N-MWCVNTs indicating the strong effect of metal nanoparticles on the improvement of the electrochemical performance of the electrodes. The variation of oxidation peak current density with the concentration of DA was found to be linear in the investigated concentration range of 0.010–0.350 mM on both N-MWCNTs and N-MWCNT/AuNP films (inset plots Fig. 3). Consequently, the lower limit of detection (*S*/*N* = 3) and the sensitivity of fabricated composite films towards DA/DAQ were estimated from the linear calibration curves and are presented in Table 2. The findings demonstrate that the sensitivity of carbon nanotubes modified with AuNPs is obviously higher. Namely, an increase up to about ~ 30% of sensitivity occurs upon modification of carbon nanotubes with AuNPs. This finding confirms that metal nanoparticles improve further the electrochemical performance of carbon nanotube–based electrodes [59]. Furthermore, the sensitivity tends to decrease slightly (about ~ 4%) in PBS solutions containing BS due probably to the uncompensated resistance effect that is more obvious in BS. Similar conclusions have been extracted from the estimated detection limits of composite films towards DA. Thus, the detection capability of carbon nanotubes tends to increase (up to about ~ 20%) upon their modification with AuNPs. Besides, the detection capability of fabricated composite films towards DA weakens slightly in BS solutions (Table 2).

Electrochemical analysis of the DA/DAQ redox system on conventional electrodes such as platinum (Pt) and glassy carbon (GC) was also carried out in BS/PBS for comparison reasons (Fig. S6; ESM). The significantly lower sensitivities estimated for Pt (0.082 A·M^{-1}·cm^{-2}) and GC (0.105 A·M^{-1}·cm^{-2}) electrodes towards DA/DAQ compared to those obtained for N-MWCNT-based films indicate the advantage of incorporating carbon nanotubes along with metal nanoparticles in electrochemical sensors. Histograms showing the comparison of sensitivities and lower limits of detection of various electrodes applied towards DA/DAQ in BS/PBS

(1:10) are presented in Fig. S7 (ESM). According to reports published in the literature, a possible mechanism for the oxidation of DA on carbon nanotubes modified with AuNPs involves π-π-interactions through the π-electron cloud of DA with the π-electron cloud of carbon nanotubes [60].

Electrochemical studies of N-MWCNTs and N-MWCNT films towards DA in PBS and BS/PBS were additionally carried out by means of the SWV technique (Fig. 4). From the linear variation of oxidation current density with the concentration on DA (inset plots Fig. 4), the sensitivity of composite films towards DA was estimated once more and compared with those obtained by means of CV technique (Table 2). The sensitivity of N-MWCNTs/AuNPs towards DA appears to be slightly greater (up to about ~ 30%) compared to that estimated for unmodified N-MWCNTs. Furthermore, the sensitivity estimated for both composite films in BS appears to be slightly smaller (up to about ~ 5%) compared to that measured in pure PBS solutions due to the uncompensated resistance effect, which is more obvious in BS solutions. These findings are in absolute agreement with those obtained by means of the CV method. It is, however, interesting to mention that the sensitivities of both N-MWCNTs and N-MWCNTs/AuNPs towards DA obtained by means of SWV appear to be about 10–15% smaller compared to those obtained using the CV technique.

The stability of N-MWCNTs and N-MWCNT/AuNP films was tested systematically for a period of 1 week, and no significant loss of electrochemical activity was observed. Anyhow, the electrochemical response (oxidation current density) after continuous use for a period of 1 week decreases at about 10–15% of the initial response. The repeatability and reproducibility of fabricated composite films were also evaluated. The reproducibility of the method was studied by measuring the electrochemical response of five different films towards DA/DAQ. In all cases, reproducibility in the range of 2.5–3.5% was estimated. Furthermore, the method's repeatability was studied by monitoring the current response of the same composite film towards DA/DAQ for 10 different successive measurements. The estimated repeatability of about 3.0% can be considered quite acceptable.

Electrochemical response of N-MWCNTs/AuNPs towards DA in the presence of AA and UA

The analysis of DA in the presence of AA and UA was carried out on N-MWCNTs and N-MWCNT/AuNP-based films by means of the CV technique to study possible interference effects. For this purpose, CVs were recorded for various concentrations of DA in the range of 0.010–0.350 mM, while the concentration of AA (0.500 mM) and UA (0.100 mM) was kept constant (Fig. 5). The estimated electrochemical parameters are presented in Table 3.

Previously published studies demonstrated that UA can be electrochemically oxidized via two-electron oxidation process to its diimine [61], while the electro-oxidation of AA to dehydroascorbic acid takes place via quasi-reversible two-electron transfer process followed by irreversible chemical reactions [62]. However, the electrochemical oxidation of AA on conventional electrodes, such as platinum (Pt) and glassy carbon (GC), requires a higher potential than the expected oxidative potential of AA; namely, it needs a so-called overpotential. The CVs recorded on N-MWCNT-based films display that the oxidation overpotential of AA (+0.005 V vs. Ag/AgCl) decreases significantly on carbon nanotubes leading to great potential separation (in the range of 200–270 mV) between the oxidation waves of AA and DA analytes preventing, thus, their overlapping. Furthermore, the separation between oxidation waves of DA and UA analytes (in the range of 115–135 mV) is enough large to prevent their overlapping and permit their simultaneous analysis. Thus, three non-overlapped (well-separated) waves corresponding to oxidation of AA (+0.005 V vs. Ag/AgCl), DA (+0.240 V vs. Ag/AgCl), and UA (+0.355 V vs. Ag/AgCl) can be clearly seen in CVs recorded on N-MWCNT-based films. The findings demonstrate a slightly greater separation between oxidation waves of studied analytes onto N-MWCNTs/AuNPs compared to unmodified N-MWCNTs confirming once more the strong effect of metal nanoparticles on the improvement of electrochemical activity of carbon nanotubes.

It is though, interesting to mention, that similar studies on Pt reveal overlapped oxidation waves for AA and DA, due to the great oxidation overpotential of AA on this particular electrode. Furthermore, quite a weak (no clear) oxidation wave has been observed for UA on the Pt electrode (Fig. S8; ESM). According to literature reports, oxidation of AA on GC and Pt electrodes requires potentials of about 0.400 vs. SCE and 0.600 V vs. SCE, respectively [63]. In the present work, the oxidation potential of +0.005 V vs. Ag/AgCl measured for AA on N-MWCNTs/AuNPs is converted to −0.040 vs. SCE (considering that SCE vs. Ag/AgCl is +0.045 V) that is significantly less anodic compared to potentials reported on GC and Pt. These observations demonstrate once more the importance of the incorporation of carbon nanotubes along with metal nanoparticles in electrochemical sensors to diminish the overpotentials of redox systems and improve their sensitivity.

From the linear variation of oxidation current density of DA with its concentration (inset plots Fig. 5), the lower limit of detection ($S/N = 3$) and the sensitivity of fabricated composite films towards oxidation of DA in the presence of AA and UA were estimated and are included in Table 3. As was expected, slightly greater sensitivity was observed for N-MWCNTs/AuNPs compared to unmodified N-MWCNTs confirming once more the strong influence of metal

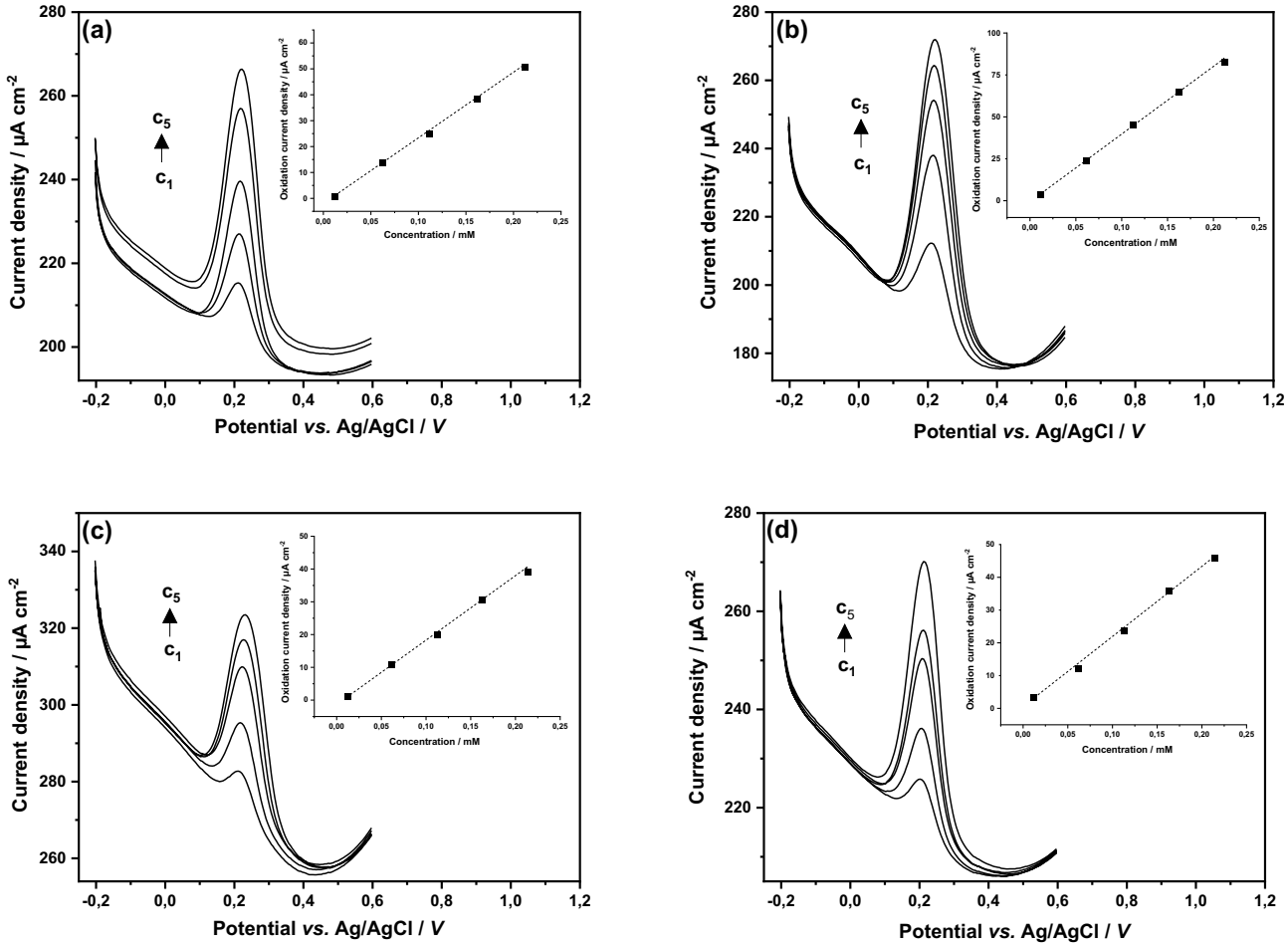

Fig. 4 SWVs recorded for various concentrations of DA in the range of 0.010–0.300 mM in PBS (**a**, **b**), BS/PBS (1:10) (**c**, **d**) on N-MWCNTs (**a**, **c**) and N-MWCNTs/AuNPs (**b**, **d**) at the scan rate of 0.02 V·s^{-1}. The insets exhibit the variation of oxidation peak current density with concentration of DA observed in recorded SWVs

nanoparticles on the enhancement of electrochemical activity carbon nanotubes. It is, however, obvious that the sensitivity of both composite films towards DA/DAQ tends to decrease somewhat (up to ~ 5%) in the presence of AA and UA (compared to sensitivity estimated for DA in the absence of AA and UA). However, this difference lies within the experimental error of the method.

It would be very interesting to compare the sensitivities of N-MWCNTs and N-MWCNTs/AuNPs towards DA/DAQ obtained in the present work with those reported in the literature for other novel composite films (Table 4) [71–85]. In general, the comparison demonstrates that both N-MWCNTs and N-MWCNTs/AuNPs exhibit in some cases greater sensitivity towards DA/DAQ compared to other novel electrodes reported in the literature. For instance, the sensitivity values estimated for glassy carbon electrode modified with either graphene (0.07 A·M^{-1}) [79] or copper oxide nanoparticles (0.04 A·M^{-1}) [81] seem to be significantly smaller compared to those obtained in the present work. Likewise, the sensitivity reported for carbon paste electrode modified with either copper oxide nanoparticles (0.29 A·M^{-1}) [82] or iron nanoparticles (0.16 A·M^{-1}) [83] appears to be smaller compared to those determined on our composite films in present work.

A further extended comparison of lower limits of detection of N-MWCNTs/AuNPs towards DA/DAQ obtained in the present work with available published values is presented in Table S1 (ESM). This comparison exhibits that the detection capability of N-MWCNTs/AuNPs appears to be either analogous or greater compared to other novel composite films. For instance, the detection limits of 52.4 µM reported for carbon paste electrode modified with poly(xylenol orange) [64], 24 µM measured for glassy carbon electrode modified with PtNPs, AuNPs, and 1-cysteine [65], and 8.0 µM published for glassy carbon electrode modified with cobalt penta-cyano-nitrosyl-ferrate [66] appear to be significantly greater, in other words, poorer, compared to those obtained on N-MWCNTs/AuNPs in the

Table 3 Oxidation peak potential difference of AA and DA analytes ($E_p^{ox}{}_{DA} - E_p^{ox}{}_{AA}$), oxidation peak potential difference of DA and UA analytes ($E_p^{ox}{}_{UA} - E_p^{ox}{}_{DA}$), lower limit of detection (*LOD*), and sensitivity (*S*) for DA/DAQ in the presence of AA (0.500 mM) and UA (0.100 mM) on N-MWCNTs and N-MWCNT/AuNP composite films in PBS and BS/PBS (1:10)

Parameters	N-MWCNTs		N-MWCNTs/AuNPs	
	PBS	BS/PBS	PBS	BS/PBS
$(E_p^{ox}{}_{DA} - E_p^{ox}{}_{AA})$ / V[a]	0.230 ± 0.006	0.203 ± 0.006	0.270 ± 0.006	0.215 ± 0.006
$(E_p^{ox}{}_{UA} - E_p^{ox}{}_{DA})$ / V[a]	0.130 ± 0.006	0.115 ± 0.006	0.135 ± 0.006	0.120 ± 0.006
LOD / μM[bc]	2.10 ± 0.07	2.80 ± 0.09	1.80 ± 0.06	2.40 ± 0.08
S / $A \cdot M^{-1} \cdot cm^{-2}$[b]	0.427 ± 0.011	0.400 ± 0.010	0.541 ± 0.014	0.505 ± 0.013

[a]All potentials are reported *versus* Ag/AgCl (saturated KCl) reference electrode

[b]The *LOD* and *S* values were estimated by means of CV technique in concentration range of 0.010–0.350 mM

[c]The *LOD* were estimated at signal-to-noise ratio of 3 (*S*/*N* = 3)

present work. In addition, the detection limits of 1.7 μM estimated for film consisting of phosphorylated zirconia-silica oxide particles modified with methylene blue [67], 1.8 μM measured for glassy carbon electrode modified with cysteine [68], and 2.3 μM obtained for glassy carbon electrode for indirect analysis based on laponite/tyrosinase [69] seem to be comparable to that measured on N-MWCNT/AuNP composite film.

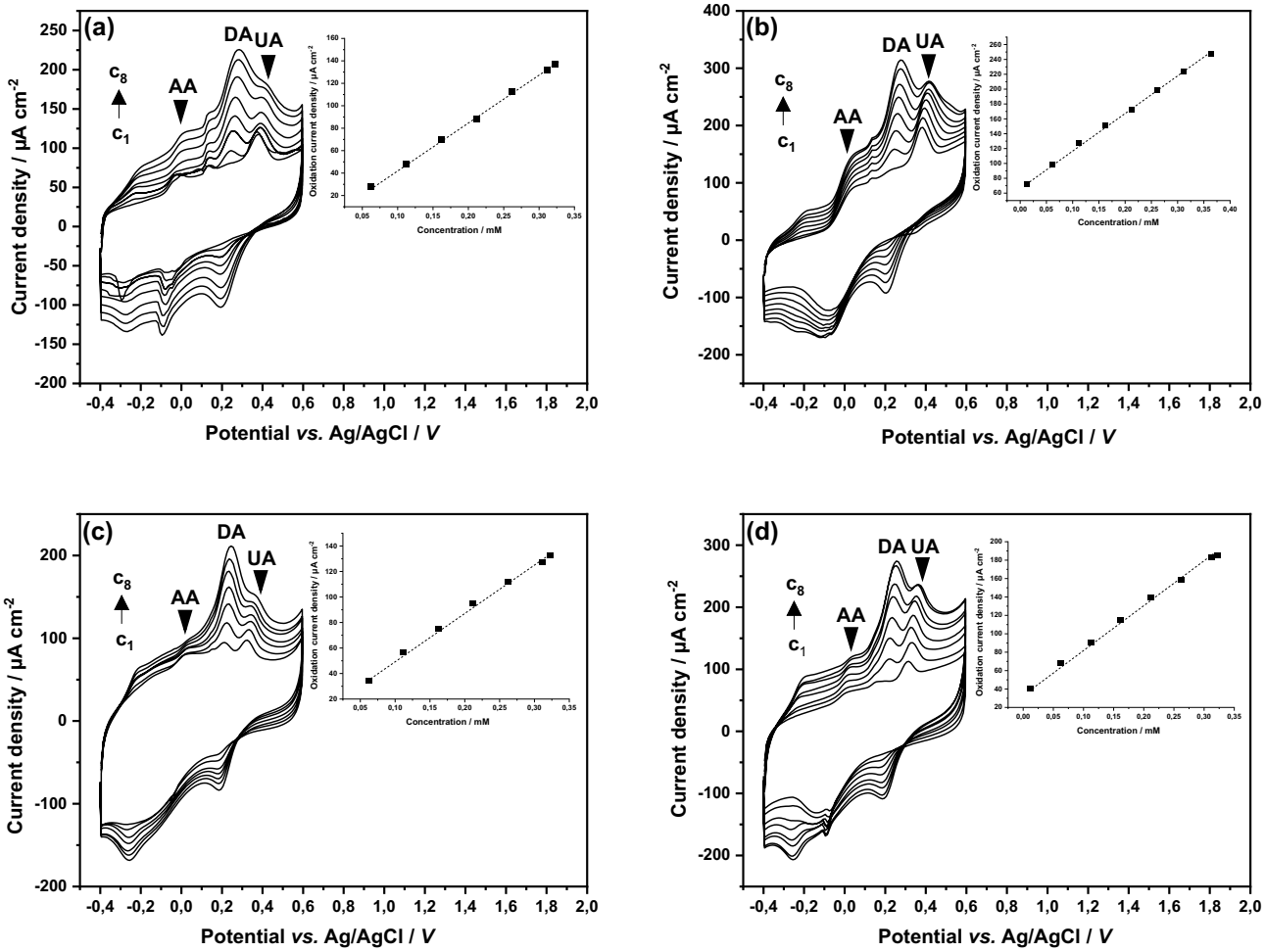

Fig. 5 CVs recorded for various concentrations of DA in range of 0.010–0.350 mM in presence of AA (0.500 mM) and UA (0.100 mM) in PBS (**a**, **b**), BS/PBS (1:10) (**c**, **d**) on N-MWCNTs (**a**, **c**) and N-MWCNTs/AuNPs (**c**, **d**) at the scan rate of 0.02 $V \cdot s^{-1}$. The insets exhibit the variation of oxidation peak current density with the concentration of DA observed in recorded CVs

Table 4 Comparison of sensitivities (*S*) obtained in present work for N-MWCNTs and N-MWCNTs/AuNPs towards DA/DAQ with those of other novel electrodes reported in literature. The sensitivities were determined by means of either cyclic voltammetry (CV), square wave voltammetry (SWV), amperometry (AMP), or differential pulse voltammetry (DPV) technique

Electrode's material	Technique	S / A·M^{-1}·cm^{-2}	Reference
N-MWCNTs[a]	CV	0.427	This work
N-MWCNT/AuNPs[a]	CV	0.541	This work
N-MWCNTs[b]	CV	0.400	This work
N-MWCNT/AuNPs[b]	CV	0.505	This work
N-MWCNTs[c]	CV / SWV	0.416 / 0.394	This work
N-MWCNT/AuNPs[c]	CV / SWV	0.548 / 0.466	This work
Pt[d]	CV	0.082	This work
GC[e]	CV	0.105	This work
Au[f]	CV	10	Ref. [71]
SWCNTs/PPy[g]	AMP	0.467	Ref. [72]
GC/PMTH[h]	DPV	1.21	Ref. [73]
Au/Pt[i]	DPV	0.50	Ref. [74]
CS/N-GQDs[j]	DPV	0.418	Ref. [75]
CPE/ZnO[k]	CV	0.42	Ref. [76]
PGE/Cu/CuxO[l]	DPV	0.51	Ref. [77]
GC/CNTs/TiO_2[m]	SWV	0.042 / 0.043	Ref. [78]
GC/GR[n]	DPV	0.07	Ref. [79]
Au[o]	DPV	0.14	Ref. [80]
GC/CuO[p]	DPV	0.04	Ref. [81]
CPE/CuO[q]	DPV	0.29	Ref. [82]
CPE/Fe[r]	DPV	0.16	Ref. [83]
GC/MIPs/CuO[s]	CV	0.27	Ref. [84]
CuO[t]	DPV	0.0229 / 0.664	Ref. [85]

[a]Values obtained in present work for DA/DAQ in presence of AA and UA in PBS

[b]Values obtained in present work for DA/DAQ in presence of AA and UA in BS/PBS (1:10)

[c]Values obtained in present work for DA/DAQ in BS/PBS (1:10)

[d]Value obtained in present work for DA/DAQ on platinum electrode in BS/PBS (1:10)

[e]Value obtained in present work for DA/DAQ on glassy carbon electrode in BS/PBS (1:10)

[f]Electrode consisting of pure gold nanoparticles

[g]Single-walled carbon nanotubes modified with poly-(pyrrole)

[h]Glassy carbon electrode modified with poly-(3-methylthiophene)

[i]Gold electrode modified with platinum nanoparticles/osmium redox polymer/Nafion

[j]Carbon screen printed electrode modified with chitosan/nitrogen-doped graphene quantum dots

[k]Carbon paste electrode modified with zinc oxide nanoparticles; *S* in A·M^{-1}

[l]Pencil graphite electrodes modified with copper/copper oxide nanoparticles; *S* in A·M^{-1}

[m]Glassy carbon electrode modified with functionalized carbon nanotubes with titanium dioxide; *S* in A·M^{-1}

[n]Glassy carbon electrode modified with graphene; *S* in A·M^{-1}

[o]Nanostructured gold electrode; *S* in A·M^{-1}

Table 4 (continued)

[p]Glassy carbon electrode modified with copper oxide nanoparticles; *S* in A·M^{-1}

[q]Carbon paste electrode modified with copper oxide nanoparticles; *S* in A·M^{-1}

[r]Carbon paste electrode modified with iron nanoparticles; *S* in A·M^{-1}

[s]Glassy carbon electrode modified with polymers and copper oxide nanoparticles; *S* in A·M^{-1}

[t]Copper oxide nanoleaf electrode; *S* in A·M^{-1}

Further additional interference studies demonstrated that norepinephrine (NEP) and glucose (GL) will probably interfere with the electrochemical analysis of DA. Namely, the peak potentials for oxidation of NEP and GL appearing at about 0.250 V (vs. Ag/AgCl) and 0.200 V (vs. Ag/AgCl), respectively, overlap with the oxidation wave of DA (0.240 V vs. Ag/AgCl). However, epinephrine (EP) and acetaminophen (AC) do not interfere with the analysis of DA. Specifically, onto N-MWCNTs/AuNPs an irreversible oxidation peak at about 0.370 V (vs. Ag/AgCl) occurs corresponding to the oxidation of EP. This oxidation peak does not overlap with that of DA that lies at about 120 mV less anodic potential. In addition, electrochemical analysis of AC on N-MWCNTs/AuNPs demonstrates that the oxidation of AC occurs at about 0.445 V (vs. Ag/AgCl), and consequently, an interference of AC in the analysis of DA cannot be expected, since DA displays an anodic wave in much less anodic potential (about 205 mV les anodic potential). As an example, representative CVs recorded for interference studies of GL in the electrochemical analysis of DA in the presence of AA and UA are reported in Fig. S9 (ESM). In these CVs, it can be clearly seen that the selective detection of DA in the presence of AA and UA cannot be carried out due to strong interference arising from the oxidation of GL.

Conclusions

N-MWCNTs were fabricated by means of CVD, decorated with AuNPs (14.0 nm), and applied for electrochemical sensing of DA in the presence of AA and UA in real BS samples. The oxidation wave of DA was not overlapped with those of AA and UA, since the oxidation overpotential of AA decreases significantly on N-MWCNT-based films. Consequently, the three well-defined CV peaks of analytes are separated enough in order to permit the successful analysis of DA in the presence of AA and UA in BS samples. N-MWCNTs/AuNPs exhibit greater sensitivity (0.505 A·M^{-1}·cm^{-2}), and accordingly, lower detection limit (2.4 μM) towards DA in the presence of AA and UA compared to unmodified N-MWCNTs (0.400 A·M^{-1}·cm^{-2}; 2.8 μM). These findings confirm the strong influence of metal nanoparticles on the improvement of the electrochemical

performance of carbon nanotube–based electrodes. Comparison with available literature data demonstrates that the sensitivity of fabricated N-MWCNT/AuNP composite films towards DA is quite enhanced permitting their future application for sensing DA in real BS samples.

Supplementary Information The online version contains supplementary material available at https://doi.org/10.1007/s10008-023-05562-2.

Acknowledgements The authors would like to thank Mrs. D. Schneider (TU Ilmenau) for the help in electrochemistry experiments, and Mr. Lars Haffermann (TU Ilmenau) for the fabrication of AuNPs.

References

1. Ranganathan S, Kuo T, McCreery RL (1999) Anal Chem 71:3574–3580
2. Sherigara BS, Kutner W, D'Souza F (2003) Electroanal 15:753–772
3. Matzui LYu, Ovsienko IV, Len TA, Prylutskyy YuI, Scharff P (2005) Fuller Nanotub Carbon Nanostructures 13:259–265
4. Ovsienko V, Len TA (2007) Matzui LYu, Prylutskyy YuI, Ritter U, Scharff P, Le Normand F, Eklund P. Mol Cryst Liq Cryst 468:289–297
5. Yun YH, Dong Z, Shanov V, Heineman WR, Halsall HB, Bhattacharya A, Conforti L, Narayan RK, Ball WS, Schulz MJ (2007) Nano Today 2:30–37
6. Zhou J, Zhang K, Liu J, Song G, Ye B (2012) Anal Methods 4:1350–1356
7. Bakır ÇC, Şahin N, Polat R, Dursun Z (2011) J Electroanal Chem 662(2):275–280
8. Song YZ, Li X, Song Y, Cheng ZP, Zhong H, Xu JM, Lu JS, Wei CG, Zhu AF, Wu FY, Xu J (2013) Russ J Phys Chem A 87:74–79
9. Wu B, Ou Z, Ju X, Hou S (2011) J Nanomat 2011:1–6
10. Huffman ML, Venton BJ (2009) Analyst 134:18–24
11. Garris PA, Wightman RM (1994) J Physiology 478:239–249
12. Wightman RM, May LJ, Michael AC (1988) Anal Chem 60:769A-793A
13. Mo JW, Ogoreve B (2001) Anal Chem 73:1196–1202
14. Sarre S, Michotte Y, Herregodts P, Deleu D, De Klippel N, Ebinger G (1992) J Chromatogr B 575:207–212
15. Guan CL, Ouyang J, Li QL, Liu BH, Baeyens WRG (2000) Talanta 50:1197–1203
16. Kang TF, Shen GL, Yu RQ (1997) Anal Chim Acta 354:343–349
17. Seçkin ZE, Volkan M (2005) Anal Chim Acta 547(1):104–108
18. Dayton MA, Ewing AG, Wightman RM (1980) Anal Chem 52(14):2392–2396
19. Tsierkezos NG, Ritter U (2012) J Solid State Electrochem 16:2217–2226
20. Kang J, Zhuo L, Xiaoquan L, Xiaoqiang W (2005) J Solid State Electrochem 9:114–120
21. Jin GP, Lin XQ, Ding YF (2006) J Solid State Electrochem 10:987–994
22. Li NB, Ren W, Luo HQ (2008) J Solid State Electrochem 12:693–699
23. Ardakani MM, Talebi A, Naeimi H, Barzoky MN, Taghavinia N (2009) J Solid State Electrochem 13:1433–1440
24. Ti CC, Kumar AS, Chen SM (2009) J Solid State Electrochem 13:397–406
25. Zhang L, Wang L (2013) J Solid State Electrochem 17:691–700
26. Shieh YT, Lu YT, Wang TL, Yang CH, Lin RH (2014) J Solid State Electrochem 18:975–984
27. Yang S, Li G, Yang R, Xia M, Qu L (2011) J Solid State Electrochem 15:1909–1918
28. Zhang L, Shi Z, Lang Q (2011) J Solid State Electrochem 15:801–809
29. Goyal RN, Gupta VK, Bachheti N, Sharma RA (2008) Electroanal 20:757–764
30. Zhang R, Jin GD, Chen D, Hu XY (2009) Sensor Actuat B Chem 138:174–181
31. Castro SSL, Mortimer RJ, de Oliveira MF, Stradiotto NR (2008) Sensors 8:1950–1959
32. De Oliveira MI, Andrade Alves W (2011) ACS Appl Mater Interfaces 3:4437–4443
33. Majewska UE, Chmurski K, Biesiada K, Olszyna AR, Bilewicza R (2006) Electroanal 18:1463–1470
34. Rekha, Swamy BEK, Deepa R, Krishna V, Gilbert O, Chandra U, Sherigara BS (2009) Int J Electrochem Sci 4:832–845
35. Huang J, Liu Y, Hou H, You T (2008) Biosens Bioelectron 24:632–637
36. Ensafi AA, Dadkhah-Tehrani S, Rezaei B (2010) J Serb Chem Soc 75(12):1685–1699
37. Farhadi K, Kheiri F, Golzan M (2008) J Braz Chem Soc 19:1405–1412
38. Zhang L, Wu J (2011) Sens Lett 9:1755–1766
39. Rao CNR, Sen R (1998) Chem Commun 1525–1526
40. Tsierkezos NG, Ritter U (2010) J Appl Electrochem 40:409–417
41. Tsierkezos NG, Szroeder P, Ritter U (2011) Fullerenes Nanotubes Carbon Nanostruct 19:505–516
42. Tsierkezos NG, Rathsmann E, Ritter U (2011) J Solution Chem 40:1645–1656
43. Köhler JM, Li S, Knauer A (2013) Chem Eng Technol 36:887–899
44. Hafermann L, Köhler JM (2015) Chem Eng Technol 38:1138–1143
45. Tsierkezos NG, Philippopoulos AI, Ritter U (2010) J Solution Chem 39:897–908
46. Tsierkezos NG, Puschner M, Ritter U, Knauer A, Hafermann L, Köhler JM (2016) Ionics 22:1957–1965
47. Tsierkezos NG, Ritter U (2011) Phys Chem Liq 49:729–742
48. Tsierkezos NG, Ritter U, Nugraha Thaha Y, Krischok S, Himmerlich M, Downing C (2015) Chem Phys Lett 639:217–224
49. Szroeder P, Tsierkezos NG, Scharff P, Ritter U (2010) Carbon 48:4489–4496
50. Katayama T, Araki H, Yoshino K (2002) J Appl Phys 91:6675–6678
51. Hawley MD, Tatawawadi SV, Piekarski S, Adams RN (1967) J Am Chem Soc 89:447–450
52. Zhu M, Huang XM, Li J, Shen HX (1997) Anal Chim Acta 357:261–267
53. Sternson AW, McCreery R, Feinberg B, Adams RN (1973) J Electroanal Chem Interfacial Electrochem 46:313–321
54. Kadish KM, Larson G (1977) Bioinorg Chem 7:95–105
55. Nicholson RS (1965) Anal Chem 37(11):1351–1355
56. Nicholson RS, Shain I (1964) Anal Chem 36(4):706–723
57. Yamaguchi T, Komura T, Hayashi S, Asano M, Niu GY, Takahashi K (2006) Electrochemistry 74(1):32–41
58. Teófilo RF, Ceragioli HJ, Peterlevitz AC, Da Silva LM, Damos FS, Ferreira MMC, Baranauskas V, Kubota LT (2007) J Solid State Electrochem 11:1449–1457
59. Fritea L, Banica F, Costea TO, Moldovan L, Dobjanschi L, Muresan M, Cavalu S (2021) Materials 14(21):6319 (37 pages)
60. Poudyal DC, Satpati AK, Kumar S, Haram SK (2019) Mater Sci Eng C 103:109788 (9 pages)
61. Owens JL, Marsh HA, Dryhurst G (1978) J Electroanal Chem 91:231–247
62. Karavidas P, Jannakoudakis D (1984) J Electroanal Chem 160(1–2):159–167
63. Karim-Nezhad G, Hasanzadeh M, Saghatforoush L, Shadjou N, Khalilzadeh B, Ershad S (2009) J Serb Chem Soc 74:581–593
64. Narayana PV, Madhusudana Reddy T, Gopal P, Reddaiah K, Raghu P (2014) Res J Chem Sci 4:37–43
65. Thiagarajan S, Chen SM (2007) Talanta 74:212–222

66. Bari MR, Sabzi RE (2008) Asian J Chem 20:3357–3363
67. Arguello J (2008) leidens VL, Magossa HA, Ramos RR, Gushikem Y. Electrochim Acta 54:560–565
68. Zhang L (2008) Microchim Acta 161:191–200
69. Menolasina S, Martín-Fernandez B, García-Iñigo FJ, López-Ruiz B (2011) Sens Lett 9:1670–1675
70. Moldenhauer J, Meier M, Paul DW (2016) J Electrochem Soc 163:H672–H678
71. Kurniawan F, Tsakova V, Mirsky VM (2009) J Nanosci Nanotechnol 9:2407–2412
72. Min K, Yoo YJ (2009) Talanta 80:1007–1011
73. Huong VT, Shimanouchi T, Quan DP, Umakoshi H, Viet PH, Kuboi R (2009) J Appl Electrochem 39:2035–2042
74. Liu C, Liu H, Yang Q, Lin N, Song Y, Wang L, Cai X (2009) Adv Mat Res 60–61:311–314
75. Ben Aoun S (2017) R Soc Open Sci 4(11):171199
76. Fooladsaz K (2012) Int J Electrochem 7:9892–9908
77. Bahrami E, Amini R, Vardak S (2020) J Alloys Compd 855(2):157292
78. Mazloum-Ardakani M, Khoshroo A (2014) Electrochim Acta 130:634–641
79. Kim YR, Bong S, Kang YJ, Yang Y, Mahajan RK, Kim JS, Kim H (2010) Biosens Bioelectron 25:2366–2369
80. Plowman BJ, Mahajan M, O'Mullane AP, Bhargava SK (2010) Electrochim Acta 55:8953–8959
81. Krishnamoorthy K, Sudha V, Kumar SM (2018) J Alloys Compd 748:338–347
82. Reddy S, Swamy BK, Jayadevappa H (2012) Electrochim Acta 61:78–86
83. Lai GS, Zhang HL, Han DY (2008) Anal Lett 41:3088–3099
84. Li B (2015) Biosens Bioelectron 67:121–128
85. Zheng Z, Qiu H, Zheng M, Weng S, Huang Z, Xian R, Lin X (2014) Anal Methods 6:7923–7927